Resonance structure in the electron-impact excitation of Ca^+ below the 5s threshold

O. I. Zatsarinny, V. I. Lengyel, and E. A. Masalovich
Uzhgorod State University, Uzhgorod, Ukraine, U.S.S.R.
(Received 30 July 1990)

Detailed calculations of energies and widths of Ca autoionizing states and the related resonance structure in electron-impact excitation of the 4s-4p transition in Ca^+ are performed using the diagonalization method. This method is divided into two steps: a three-state (4s,3d,4p) close-coupling calculation of cross sections and extensive configuration-interaction calculations of wave functions of autoionizing states. Both steps take into account the correlations related to one- and two-body core-polarization potentials. The results of calculations of energies, oscillator strengths, and autoionizing widths of doubly excited states of Ca are in better agreement with the experimental data than any other calculation. Rich resonance structure is predicted by theory at incident electron energies below the 5s threshold. The present results support the general pattern of the measurements of Frontov [Opt. Spectrosc. **9**, 460 (1985)], although there are some discrepancies in the details, particularly the existence of the high and broad resonance at that threshold. A detailed comparison with the previous resonance calculations by Mitroy *et al.* [Phys. Rev. A **38**, 3339 (1988)] is carried out.

PACS number(s): 34.80.Kw

I. INTRODUCTION

The development of experimental techniques in recent years has rendered the detailed study of scattering cross sections of electrons by positive ions and particularly their resonance structure increasingly practicable. This structure is caused by the capture of an incident electron by the excited-ion target into short-lived autoionizing states (AIS's), the further Auger decay of which leads to a sharp variation in the scattering cross section. In recent years great attention has been paid to the study of resonance structure in the scattering cross section, because the latter is a source of information on the structure of atoms. It allows one to carry out a more careful selection of theoretical models for describing the scattering processes. In applications, resonances often lead to a noticeable increase of the corresponding velocities of reactions.

The experimental study of the resonance structure in ion cross sections is a difficult task, because highly monochromatic electron beams are needed. For this reason the number of such investigations is limited. The ions of alkaline-earth metals make convenient vehicles for carrying out precise investigations using monoenergetic beams of electrons of small intensity. Indeed, for these ions the spectral transitions from the lower levels fall into the conveniently visible spectral region. Moreover, the excitation cross sections for lower levels are comparatively high ($\sim 10^{-15}$ cm^2). That is why as far back as the 1970's a number of laboratories had carried out experimental investigations of excitation cross sections for different transitions in the ions of alkaline-earth metals. In particular, thorough measurements of the 4s-4p excitation cross section in Ca^+ were carried out by Taylor and Dunn [1], whose results were later confirmed by the measurements of Zapesochnyi *et al.* [2]. In addition, Zapesochnyi *et al.* also published cross-section data for exciting 5s and 4d levels from the ground state, which were important for estimating the population of the 4p level by cascading. The most interesting result of these measurements is the considerable discrepancy in the near-threshold region between experiment and calculation for the 4s-4p transition. For example, the difference between experiment and the most exact calculations at that time, in the close-coupling method (CCM) by Burke and Moores [3], reaches about 35%. Nevertheless this has not stimulated further interest in the theoretical study of this transition, and until recently only Coulomb-Born and distorted-wave [4–6] calculations were carried out and agreement with experimental data was reached only for high energies of the projectile electron.

Only very recently, in attempts to explain the experimental data, have more rigorous methods been applied. With the aim of accounting for contributions from cascading, Msezane [7] carried out close-coupling calculations of three (3CC) and six (6CC) low-lying states using an exact target wave function. However, these calculations did not noticeably improve agreement with experiment. Moreover, a 6CC expansion gives even bigger cross sections than the 3CC expansion. At the same time Mitroy *et al.* [8] carried out detailed calculations of excitation cross sections for Ca^+; their most exact model—6CC calculations with exact semiempirical Hartree-Fock (HF) target wave functions—agrees better with experimental data than any of the previous calculations. This, up to now, has been the only work in which resonance structure has been included. However, if cascading from 5s, 4d, and 5d levels is taken into account, then the 6CC cross-section excitation exceeds the experimental data by 20% [9].

Unfortunately, the very interesting experimental work of Frontov [10] turned out to be outside the scope of the above-mentioned theoretical investigations. Frontov resolved the resonance structure in the 4s-4p excitation cross section of Ca^+ by using more monoenergetic elec-

tron beams ($\Delta E=0.15$ eV in the near-threshold region). This method revealed unexpectedly high resonance peaks, and the measured near-threshold excitation cross section considerably exceeded both the previous experimental measurements [1,2] and the calculations of Mitroy *et al.* [8], especially near threshold.

In the present work, the calculations using the diagonalization method (DM) were carried out with the aim of interpreting the measured resonance structure of the excitation cross section for the $4s$-$4p$ transition in Ca^+. The method was proposed by Balashov *et al.* [11] for the study of the resonance photoionization of atoms, and later it was successfully used for the description of resonance structure in electron collision cross sections with "one-electron" targets like He^+ [12], Be^+ and Mg^+ [13], and light alkaline-metal atoms [14]. One advantage of this method is the possibility of a detailed investigation of resonance structure. Below, in Sec. II, the properties of the DM are outlined, in Sec. III the bound-state wave functions of Ca^+ are described, in Sec. IV results on the nonresonant excitation cross section are presented, and in Sec. V the results for AIS parameters are given. The results of our calculations of resonance structure for the $4s$-$4p$ transition are presented in Sec. VI, where we also compare them with other work. In this paper atomic units are used.

II. DIAGONALIZATION METHOD

We describe only the main features of our variant of the diagonalization method that directly concern our calculations. A more detailed description of the DM can be found in other initial work [11–13,15].

Electron scattering on an N-electron atomic target is reduced to the solving of the Schrödinger equation

$$(H-E)\Psi(\Gamma X,x_{N+1})=0\ , \tag{2.1}$$

with appropriate boundary conditions. The collision wave function $\Psi(\Gamma X,x_{N+1})$ presents a fully antisymmetrized wave function of the system "target plus projective electron," where $X=(x_1,\ldots,x_N)$, $x_i=(r_i,\sigma_i)$ with spatial (r_i) and spin (σ_i) coordinates of the electron i, and Γ is a complete set of quantum numbers of the $(N+1)$-electron system. A nonrelativistic Hamiltonian H has been used.

As in the close-coupling method, the total wave function of the system in the DM is presented by way of expansion on wave functions of the target. But in the DM, in this expansion only those terms that correspond to the open channels are retained, whereas closed channels and electron capture are accounted for by AIS wave functions, which are usually multyconfigurational functions satisfying the condition

$$\langle\chi_\mu|H|\chi_\nu\rangle=\varepsilon_\mu\delta_{\mu\nu}\ . \tag{2.2}$$

Then the initial expansion of the collision wave function in the diagonalization approach has the form

$$\Psi(\Gamma X,x_{N+1})=(N+1)^{-1/2}\sum_{p=1}^{N+1}(-1)^{N+1+p}\sum_{\Gamma'}\Psi(\Gamma' X,\hat{r}_p\sigma_p)\frac{F_{\Gamma\Gamma'}}{r_p}+\sum_\mu C_\mu^\Gamma\Phi_\mu(\Gamma x_1,\ldots,x_{n+1})$$
$$+\sum_\nu\Lambda_\nu^\Gamma\chi_\nu(\Gamma x_1,\ldots,x_{N+1})\ , \tag{2.3}$$

where the summation over Γ is carried out over open channels exclusively. As in the conventional CCM, a set of single-configurational so-called correlational functions $\Phi(x_1,\ldots,x_{N+1})$ is added in the expansion. These functions compensate for the usual orthogonality condition for radial wave functions of the projectile electron $F_{\Gamma\Gamma'}(r)$ with the atomic orbitals of the target $P_{nl}(r)$. The functions $F_{\Gamma\Gamma'}(r)$ and coefficients Λ_ν^Γ and C_μ^Γ are the unknown quantities in the problem.

The calculation of the functions χ_ν is usually based on the configuration-interaction (CI) method, in which the functions χ_ν are constructed as linear combinations of single-configuration $(N+1)$-electron wave functions, and configuration-mixing coefficients are found from the condition (2.2). In isolation, the functions χ_ν and their eigenenergies ε_ν may be seen as wave functions and energies of AIS's in approximation. In the DM they are then coupled to the open channels in first-order perturbation theory, which gives rise to an energy shift of the AIS's and to a finite lifetime for these states.

Let us note that expansion (2.3) incorporates the closed channels only approximately, since the functions χ_ν decrease exponentially with respect to all the variables, while the functions $F_{\Gamma\Gamma'}$ in the CCM may decrease far more slowly; e.g., in a power-law fashion. For this reason, probably, the polarization of the ion by the incident electron is incorporated in a slightly poorer way by expansion (2.3) than in the CCM.

On the other hand, the DM yields more accurate parameters of the autoionizing states, since one can easily extend the wave-function basis, from which the χ_ν are constructed. We shall see an example of this situation in what follows.

Applying the variational principle mentioned above to the function (2.3) (both the function $F_{\Gamma\Gamma'}$ and the coefficients Λ_ν^Γ and C_μ^Γ are to be varied), we find the following system of coupled algebraic-integro-differential equations for determining these quantities (replacing the channel indices Γ,Γ' by the indices i,j, etc.):

$$\sum_j\mathcal{L}_{ij}F_{jj'}+\sum_\mu C_\mu^{j'}V_{i\mu}^c+\sum_\nu\Lambda_\nu^j U_{i\nu}+\sum_\lambda m_\lambda P_{n_2l_2}\delta_{l_il_\lambda}=0\ , \tag{2.4}$$

$$\sum_{\nu}(H_{\mu\nu}-E\delta_{\mu\nu})C_{\nu}^{j'}+\sum_{j}\int V_{i\mu}^{c}F_{jj'}dr+\sum_{\nu}W'_{\mu\nu}\Lambda_{\nu}^{j}=0\ , \tag{2.5}$$

$$(\varepsilon_{\mu}-E)\Lambda_{\nu}^{j'}+\sum_{j}\int U_{j\mu}F_{jj'}dr+\sum_{\nu}W'_{\mu\nu}C_{\nu}^{j'}=0\ , \tag{2.6}$$

where

$$\mathcal{L}_{ij}=-\frac{1}{2}\left[\frac{d^2}{dr^2}-\frac{l_i(l_i+1)}{r^2}+\frac{2Z}{r}+K_i^2\right]\delta_{ij}+V_{ij}+W_{ij}\ . \tag{2.7}$$

V_{ij} is the direct interaction potential of the colliding electron with the target, while W_{ij} is the corresponding exchange potential. The functions $U_{i\mu}, V_{j\mu}^{c}$ depend on the particular atom or ion chosen and they are matrix elements of the Coulomb interaction between the functions Φ_{μ} and the target wave functions. Explicit expressions for these potentials are given, e.g., by Smith and Morgan [16].

To solve the system (2.4)–(2.7), we make a first assumption; namely, we neglect the interaction of AIS's with the states described by correlation functions Φ_{μ}, i.e., we put $W'=0$. This seems to be completely justified, since W' is a matrix element of the Coulomb interelectron interaction between the states, the wave functions of which weakly overlap. Then Eqs. (2.5) and (2.6) decouple (it should be noted that indirect coupling of these equations remains due to the functions of the continuum F_{ij}). Solutions of Eqs. (2.4)–(2.7) can be found in the form

$$F_{ij}(r)=F_{ij}^{0}(r)-\sum_{\nu}\sum_{j'}\int dr'G_{ij'}(r,r')U_{j'\nu}(r')\Lambda_{\nu}^{j}\ , \tag{2.8}$$

where F_{ij}^{0} is a regular solution of the system (2.4)–(2.7) without the right-hand part, and $G_{ij}(r,r')$ is a corresponding Green matrix. If one substitutes (2.8) in (2.5) and makes the main "diagonalization" assumption, neglecting off-diagonal elements,

$$\int dr\,dr'U_{i\mu}(r)G_{ij}(r,r')U_{i\nu}(r'),\quad \nu\neq\mu \tag{2.9}$$

one obtains the expressions for Λ_{μ} and F_{ij} at once,

$$\Lambda_{\mu}=\frac{(U_{\mu}|F^{0})}{E-\varepsilon_{\mu}+\bar{\Delta}_{\mu}}\ , \tag{2.10}$$

$$\bar{\Delta}_{\mu}=-(U_{\mu}|G|U_{\mu})\ , \tag{2.11}$$

$$F_{ij}(r)=F_{ij}^{0}(r)+\sum_{\nu}\sum_{j'}\int dr'G_{ij'}(r,r')U_{j\nu}(r')\frac{(U_{\mu}|F^{0})}{E-\varepsilon_{\mu}+\bar{\Delta}_{\mu}}\ . \tag{2.12}$$

The "diagonalizational" assumption is the only essential simplification in our approach compared to Feshbach's method, because the direct coupling of the open and closed channels is accounted for exactly in the framework of the chosen basis for this set of channels, and only the coupling of different autoionizing levels through open channels is not involved.

Asymptotic solutions of (2.12) yield the K matrix, and it follows from relations between the K and T matrix that

$$T_{ij}=T_{ij}^{0}+2i\sum_{\mu,\nu}(\alpha_{\mu i}\alpha_{\mu j})\left[E-e-\Delta+\frac{i}{2}\Gamma\right]^{-1}_{\mu\nu}\ , \tag{2.13}$$

where T_{ij}^{0} are matrix elements of nonresonant scattering, and the second term describes resonance scattering. It is the generalization of the Breit-Wigner formula to the multichannel case. The possibility of explicitly singling out this resonance part is an important advantage of the DM. The quantities T_{ij}^{0} as well as the quantities $\alpha_{\mu i}$, Δ_{μ}, and Γ_{μ} are expressed in terms of the solutions F_{ij}^{0} of the system (2.4)–(2.7) without its right-hand side, i.e., the solution of the system of CCM equations neglecting closed channels. Quantities appearing in (2.13) have the following form (in our notation greek indices mark AIS's, latin indices the channels; in addition, at each fixed μ, α_{μ} is a vector whose dimension is equal to the number of open channels)

$$\alpha_{\mu}=(1-iK^{0})^{-1}\gamma_{\mu},\quad (\gamma_{\mu})_{i}=\sum_{j}\int dr\,F_{ij}^{0}(r)U_{j\mu}(r)\ , \tag{2.14}$$

$$\Gamma_{\lambda\mu}=2(\alpha_{\lambda},\alpha_{\mu}),\quad \Delta_{\lambda\mu}=(\alpha_{\lambda},K^{0}\alpha_{\mu})\ , \tag{2.15}$$

$$e_{\lambda\mu}=(\varepsilon_{\mu}-\bar{\Delta}_{\mu})\delta_{\lambda\mu},\quad E_{\lambda\mu}=E\delta_{\lambda\mu}\ . \tag{2.16}$$

The quantities Δ_{μ} give the shift of the resonant energies ε_{μ} due to the interaction of the discrete states χ_{μ} with the adjacent continuum. The total width of the resonance is

$$\Gamma_{\mu}=\sum_{i}\Gamma_{\mu i},\quad \Gamma_{\mu i}=2|\alpha_{\mu i}|^{2}\ , \tag{2.17}$$

where $\Gamma_{\mu i}$ is the partial width of resonance μ due to decay into channel i.

Thus the DM is quite a bit less laborious in comparison to the CCM for solving resonance scattering problems for slow electrons by atoms and ions. In practice it is divided into a number of simpler successive steps: solution of the CCM system only for open channels at a small number of projectile electron energies; calculation of the wave functions of AIS's and their parameters; and, finally, calculation of the resonance scattering cross section. An application of this method to the $4s$-$4p$ transition in Ca^{+} is presented in the following sections.

III. Ca^{+} BOUND-STATE WAVE FUNCTIONS

Calculations of scattering processes crucially depend upon the quality of target wave functions. In spite of the simple one-electron character of the Ca^{+} wave function, the usual one-configuration HF calculations lead to considerable errors, which is a consequence of the large dipole polarizability of the Ca^{2+} core. Because it is convenient to have the same set of one-particle radial orbitals for all considered states (both bound and AIS), we have chosen target wave functions of the frozen-core type with a semiempirical polarization potential. First, core wave functions are obtained in the HF approximation. These functions are not changed in all further calculations. Then, wave functions of the valence electron are calculated with the use of the modified one-electron Hamiltonian,

$$H^{(1)}=H^{\mathrm{HF}}+V_{\mathrm{pol}}\ , \tag{3.1}$$

where H^{HF} is Hartree-Fock Hamiltonian for the valence electron, and V_{pol} is the model potential, which takes into account the polarization of the core by the outer electron. The latter is chosen in the form initially adopted by Norcross and Seaton [17],

$$V_{\mathrm{pol}}(r,l)=-\frac{\alpha_d}{2r^4}\left[1-\exp\left[-\frac{r^G}{\rho_l^6}\right]\right]\ . \tag{3.2}$$

Here α_d is the dipole polarizability of the core of $3.16a_0^3$ [18], ρ_l are the adjustable parameters that depend on the orbital momentum of the valence electron l. These parameters were chosen in such a way that ionization energies of valence electrons reproduce experimental values (averaged over fine-structure levels). One obtains values for ρ_l of $1.545a_0$, $1.5797a_0$, $1.8633a_0$, and $1.633a_0$ for $l=0$, 1, 2, and 3.

For HF calculations we have modified the MCHF-77 program [19] in order to account for the polarization of the core. The values obtained differ slightly from those of Mitroy *et al.* [8], because they use analytical HF wave functions and frozen-core orbitals obtained from $Ca^+(3p^64s)$, instead of $Ca^{2+}(3p^6)$ in the present work. We note that the crude value $\alpha_d=3.45a_0^3$ [20] in our previous work [9] had led to a considerable difference in value for ρ_l, but in the final results for the scattering cross section this made only a slight difference in the fourth digit, which is comparable with calculational errors. We conclude that the polarization potential V_{pol} depends only weakly on the chosen value α_d. In an attempt to estimate the accuracy of our target wave functions, we present in Table I the experimental and theoretical ionization energies for low-lying states of Ca^+ obtained in different approximations. Fully self-consistent and frozen-core HF ionization energies are good in all cases, except for $3d$, probably because $3d$ orbitals penetrate deeply into the atomic core. For the same reason the $3d$ orbital is much more sensitive to the polarized core potential, and that leads to an anomalously large value of ρ_2. We may conclude that, in general, the frozen-core approximation is justified, and that it is unlikely to lead to large errors in the scattering calculations. As seen in Table I the ionization energies with semiempirical valence orbitals are in agreement with experiment to within 1%, which is much better than the uncertainty in HF calculations of 5%. Good agreement is obtained also with the analogous calculations of Mitroy *et al.* [8]. Differences for $5s$ binding energy have already been explained by the frozen-core choice. The largest discrepancy with experiment occurs for $4d$ orbitals and is caused by the behavior of $3d$ orbitals and anomalously large ρ_2 values. It should also be noted that binding energies for high-lying valence orbitals (up to $n=14$) are equally good, indicating that the chosen model for describing core polarization effects for all valence orbitals may also be adequate in the case of continuum orbitals.

The polarization potential model is widely used at present (Laughlin and Victor [22]). It aims at simulating correlation and, to some degree, relativistic effects, for core–valence-shell interaction. Oscillator strengths are particularly sensitive to the accuracy of valence orbital wave functions. In Table II we compare oscillator strengths calculated in the HF approximation with those calculated in a core-polarization potential approach and with experimental data. The oscillator strengths are presented in the length form f_L and in the velocity form f_V.

At high core polarizability, the influence of indirect radiative effects is large and may be accounted for by a modification of the radial part of the dipole operator, proposed by Bersuker [23] on the basis of the core model, as the dielectric sphere with polarizability α_d,

$$D_L(nl\rightarrow n'l')=\varphi(r) =r\left\{1-\frac{\alpha_d}{r^3}\left[1-\exp\left[-\frac{r^6}{\bar{\rho}^6}\right]\right]^{1/2}\right\}\ . \tag{3.3}$$

The corresponding modification for the velocity form is

$$D_V(nl\rightarrow n'l') =\frac{1}{\Delta E}\left[\varphi'\frac{d}{dr}+\frac{l'(l'+1)-l(l+1)}{2r^2}\varphi+\frac{\varphi''}{2}\right]\ , \tag{3.4}$$

where ΔE is the transition energy; φ' and φ'' are the corresponding derivatives on r; $\bar{\rho}=(\rho+\rho')/2$; and in ex-

TABLE I. Theoretical and experimental binding energies (in rydbergs) for the low-lying valence states of Ca^+.

State	Related core	Fixed $3p^6$ core	Fixed $4s$ core+V_{pol} [a]	Fixed $3p^6$ core+V_{pol}	Expt.[b]
$4s$	0.831 318	0.830 082	0.872 556	0.872 555	0.872 556
$3d$	0.688 196	0.666 160	0.747 836	0.747 836	0.747 835
$4p$	0.618 748	0.618 549	0.641 642	0.641 641	0.641 640
$5s$	0.385 714	0.385 630	0.396 064	0.396 791	0.397 175
$4d$	0.339 084	0.338 379	0.350 302	0.350 345	0.354 492
$5p$	0.313 020	0.312 997	0.320 132	0.320 170	0.320 460
$4f$	0.250 354	0.250 354	0.252 376	0.252 376	0.252 376

[a]Reference [8].
[b]Reference [21].

TABLE II. Absorption oscillator strengths for transitions among the low-lying valence states of Ca^+.

	Ab initio HF[a]		HF+V_{pol}				
Transition	f_L	f_V	f_L	f_V	f_L[a]	f_L[b]	Expt.
4*s*-4*p*	1.092	1.032	0.960	0.912	0.961	1.100	0.99±0.03[c] 1.05±0.09[d]
4*s*-5*p*	$<10^{-4}$	0.0001	0.0017	0.0025	0.0019	$<10^{-4}$	
4*p*-5*s*	0.173	0.165	0.179	0.173	0.179	0.173	0.18±0.02[d]
5*s*-5*p*	1.516	1.479	1.486	1.464	1.477	1.520	
3*d*-4*p*	0.049	0.0065	0.067	0.031	0.066	0.075	0.053±0.006[c]
3*d*-5*p*	0.0001	0.0005	0.0004	$<10^{-4}$	0.0004	0.0009	
4*p*-4*d*	0.865	0.800	0.867	0.822	0.869	0.899	0.87±0.09[d]
4*d*-5*p*	0.165	0.129	0.176	0.150	0.176	0.178	

[a]Reference [8].
[b]Using unmodified dipole operator.
[c]Reference [24].
[d]Reference [25].

pression (3.3) the same cutoff factor, which agrees with the corresponding factor for V_{pol}, is chosen.

Table II shows that a polarization potential considerably improves the accuracy of the oscillator strengths in length form compared with HF values, especially for 3*d*-4*p* transitions. In the case of 4*s*-4*p* transitions this effect is not so obvious because of competing changes in ΔE, whereas the radial dipole elements change considerably. On the other hand, the dipole matrix elements in velocity form change insignificantly and the corresponding oscillator strengths are in worse agreement with experimental data, i.e., the use of a polarized core potential improves the wave functions for valence electrons mainly at large distances from the nucleus, just in the region that is the most significant for electron-ion scattering. Table II also shows very good agreement with the results of Mitroy *et al.* [8], despite the fact that a different frozen core was used. In order to investigate the direct effect of core polarization expressed by modification (3.3), in Table II f_L values are also presented for calculations without that modification. As is seen, in most cases this direct effect predominates over the indirect effect of core polarization in oscillator strengths. In general, comparison of the ionization energies and oscillator strengths with experimental data indicates the high accuracy of calculated wave functions of the target.

IV. CALCULATION OF NONRESONANT SCATTERING

Wave functions of nonresonant scattering F_{ij}^0 and the corresponding transition matrices T_{ij}^0, for application of the DM, were calculated within the framework of the CCM, using the program IMPACT [26]. In these calculations only open channels have been considered, and in close-coupling expansion only three states of ions (4*s*, 3*d*, and 4*p*) have been included. The sum over correlational functions Φ_μ in expansion (2.3) contains all functions necessary for accounting for orthogonality. The angular coefficients, which specify the concrete type of potential in (2.4)–(2.7), were obtained with the help of our program ATEQNS. This program is based on the method of Fano [27], uses the algorithmic approach of Burke [28] and Hibbert [29], and is highly automated. Calculations within the framework of the CCM were carried out for all partial waves with $L \leq 12$ with full exchange. The contributions of the partial cross sections with $L > 12$ were evaluated in the Coulomb-Born approximation.

Core polarization (3.2) by the projectile electrons was also included in the close-coupling equations, using the same parameters ρ_l as those for the bound states, with the exception of ρ_2, the anomalously large value of which is associated with strong penetration of 3*d* orbitals into the core field. By contrast, a projectile orbital does not penetrate the core. Following the work of Mitroy *et al.* [8], the value 1.7049 for the parameter ρ_2 was therefore used, which was obtained by adjusting the binding energy of 4*d* orbital, since this orbital penetrates the core much less. The system of close-coupling equations also contains the so-called dielectronic polarization potential

$$V_{\text{diel}}(r_1,r_2)=-\frac{\alpha_d \hat{\mathbf{r}}_1\cdot\hat{\mathbf{r}}_2}{r_1^2\cdot r_2^2}\left[1-\exp\left[-\frac{r_1^6}{\bar{\rho}^6}\right]\right]^{1/2}\times\left[1-\exp\left[-\frac{r_2^6}{\bar{\rho}^6}\right]\right]^{1/2}, \tag{4.1}$$

where $\bar{\rho}=(\rho_1+\rho_2)/2$. This potential is included to account for the influence of mutual polarization of the core by valence and projectile electrons.

In Fig. 1 we compare calculated excitation cross sections for the emission line $4p_{3/2}$-$4s_{1/2}$ in Ca^+ with previous results. The calculated cross sections were multiplied by a factor of $(0.946)^{\frac{2}{3}}$ which takes into account both the spin-orbit splitting of the 4*p* level and the branching factor by radiative decay. In Fig. 1 we did not show excitation cross sections obtained to first order of perturbation theory, since all these cross sections largely overestimate the cross section in our energy range.

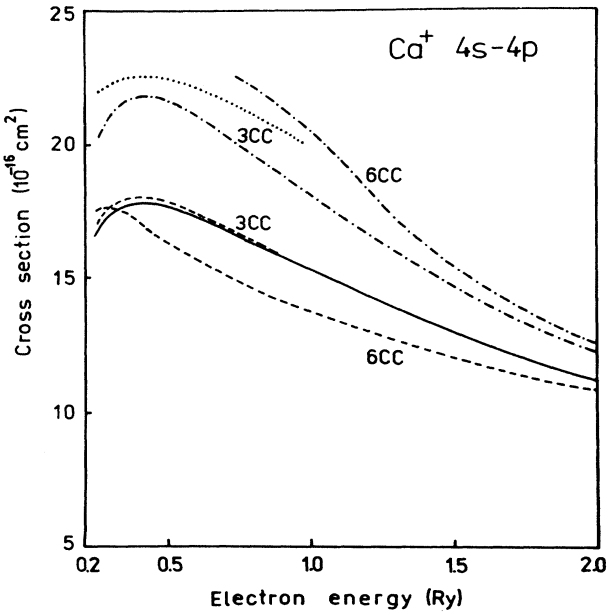

FIG. 1. Comparison of close-coupling calculations of cross sections for electron-impact excitation of the Ca^+ level: ——, 3CC, present results; · · · ·, 3CC model, Burke and Moores (1968); —·—·—·, 3CC and 6CC models, Msezane (1988); — — —, 3CC and 6CC models, Mitroy *et al.* (1988) (without resonance structure).

According to Fig. 1, our calculations agree with the 3CC calculation of Ref. [8], which uses the same approximation. Moreover, good agreement is obtained not only for total excitation cross sections of the $4s$-$4p$ transitions, but also for all partial waves up to $L=12$. Insignificant differences at threshold are caused by the indicated differences in the target wave functions. From Fig. 1 it follows that all calculations with core polarization give cross sections that are much smaller than those without; and as discussed later, agreement with experiment improves considerably. Thus, in the case of Ca^+ (and also as is shown in Ref. [9] for other heavy alkaline-earth ions) for obtaining the exact cross sections the necessary condition is the inclusion of core polarization; for example, in a simple form (3.2).

One qualitative difference between two available 6CC calculations should be noted. Figure 1 shows that the 6CC excitation cross section for the $4s$-$4p$ transition around the ionization threshold of the Ca^+ ion without core polarization [7] is 10–15 % higher than the corresponding 3CC cross section. On the other hand, the 6CC cross section with core polarization [8] is 10–15 % lower than the corresponding 3CC cross section. Different target wave functions may be the cause. However, we could not verify this assumption because our computers are too small for 6CC calculations.

V. CALCULATION OF PARAMETERS OF AUTOIONIZING STATES

We also applied the frozen-core approximation for calculating the wave functions χ_μ and the energies ε_μ of AIS's along with the configuration-interaction method in order to obtain full consistency with the calculations for the nonresonant part of the scattering process. In this approximation a complete wave function of the atom is expanded over the basis functions in which only orbitals of valence electrons change,

$$\chi_\mu^{LS}=\sum_{i=\{nl,n'l'\}} C_i\Phi_i^{LS}(\text{core},nln'l') \ . \tag{5.1}$$

Calculations have been carried out in LS coupling, which is quite applicable in the case of Ca. The set of one-particle valence-electron orbitals, of which the basis functions in expansion (5.1) were built, was obtained in the same manner as in the target case: from HF calculations of corresponding states having a single ion with a frozen core and with the use of a polarized potential with the same parameters ρ_l. This set includes up to 50 orbitals with quantum numbers $n\leq 14$ and $l\leq 3$, and was not changed in the process of all calculations. Thus our approximations reduce the calculation of AIS's of Ca to the simpler analogous case of the two-electron system.

The energies ε_μ and corresponding expansion coefficients C_i were obtained by diagonalizing the complete nonrelativistic Hamiltonian on that basis, accounting for dielectronic polarization. The basis dimension varied within 50–60 functions and it was sufficient for stabilization of 6–8 lower states of each Rydberg series of AIS's. The set of functions in each basis was chosen in such a way as to match analogous calculations in the 6CC approximation. That is, states with $4snl$, $5snl$, $4dnl$, and $5pnl$ configurations were always included, and even higher-lying configurations were included when the dimension of the basis allowed. Taking a sufficiently large set of one-particle orbitals, we can quite exactly describe the correlation between valence electrons, but the correlation between core and valence electrons still remains unaccounted for. In Ca the core is multielectronic and therefore such a correlation is important. In order to avoid certain shortcomings of the frozen-core approximation, its total energy was taken as the matching point, and the excitation energies of AIS's relative to the ground states of Ca^{2+} and Ca^+ were calculated using experimental ionization energies (11.872 and 6.113 eV for Ca^+ and Ca, respectively).

The above-described method of calculation of the AIS's is an extended variant of the restricted diagonalization method, which was introduced by Lipsky and Russek [30] to calculate the AIS's of He-like ions. However, it is difficult to apply this method when the overlap AIS series converge to different thresholds. These difficulties arise from nonphysical levels, which are sensitive to the choice of basis and usually located above the corresponding excitation threshold of the ion. They originate in the finiteness of the basis, which does not allow for a correct description of high-lying orbitals nl of the outer valence electron in the screened-core field. In the simplest case of the term ^1S of Ca, three series of $4sns$, $3dnd$, and $4pnp$ overlap and strongly interact, and it is necessary to consider them simultaneously. But it cannot be done directly because the nonphysical levels of the $4sns$ series are located in the region of the $3dnd$ and $4pnp$

TABLE III. Excitation energies and ground-state absorption oscillator strengths of the ^1P states in Ca below the $4s$ threshold.

	Energies (eV)			f_L, f_V (100)			
	Theory		Expt.		Theory		Expt.
Level	Present	Ref. [32]	Ref. [33]	Present	Ref. [32]	Ref. [34]	Ref. [35]
$4s4p$	2.956	3.053	2.932	173–162	189–182	182	175
$4s5p$	4.571	4.606	4.554	0.12–0.03	1.74–1.51	0.85	0.09
$4s6p$	5.192	5.238	5.167	2.99–2.90	0.16–0.18	1.82	4.1
$3d4p$	5.478	5.542	5.447	5.54–5.09	0.80–0.77	4.89	6.6
$4s7p$	5.652	5.710	5.632	3.78–3.09	1.10–1.04	4.09	3.2
$4s8p$	5.773	5.815	5.762	1.54–1.32	1.12–1.04	2.90	1.2
$4s9p$	5.856	5.883	5.850	0.71–0.59	1.02–0.93		0.55

series. These levels have a number of characteristic peculiarities: corresponding eigenfunctions are made up of rather large lower components, there is no dominant component, and on increasing the basis dimension the composition of the eigenfunctions and the associated eigenenergies change at random and do not converge to any fixed value. So these levels (e.g., of $4sns$ series) will interact chaotically with the levels of higher series (e.g., $3dnd$ or $4pnp$), which will lead to considerable errors for the latter. If the excitation thresholds of different series coincide or differ much in energy, as for He-like ions, then the nonphysical levels cause no trouble.

The nonphysical levels can be excluded by a two-step diagonalization. In a first step we diagonalize submatrices associated with one series. Then a new basis is built, excluding levels with "positive" energies. For lower levels of the series, the result obtained then converges rapidly and does not depend further upon the basis dimension. However, Robaux [31], analyzing details on energy and oscillator strengths for some transitions in Ca, found that the interaction with the continuum is accounted for by a "hidden" way due to nonphysical states in the restricted diagonalization method. Therefore we have tried drop as few nonphysical states as possible, the AIS's among different thresholds were considered separately and only those nonphysical levels that fall into the considered region of energies were excluded. This increases the size of the calculations insignificantly but allows one to obtain more rigorous results.

The accuracy of obtained AIS parameters is illustrated in Tables III and IV comparing calculated energies, oscillator strengths, and widths of the ^1P series of Ca with experiment. According to Table III, the energies of lower states of the series are accurate to within 0.01–0.03 eV, which is also typical for the accuracy of the AIS energies in Table IV. The largest error of the energy and other AIS parameters is encountered in the so-called perturber levels, which belong to higher-lying AIS series but lie in the same energy region as the levels of the observed series, e.g., the $3d4p$ and $4p5s$ levels of Ca, which greatly perturbs the $4snp$ and $3dnp$ series. For such levels strong configuration mixing is characteristic, they diffuse over series, and their parameters are most sensitive to the method and details of the calculation. As Table III shows, our oscillator-strength calculations are in good agreement with experimental data, and for lower states better results are obtained in the length form f_L, while for highly excited states they are obtained in the velocity form f_V [all values were calculated with the help of modified dipole operators (3.3) and (3.4)]. Besides, the calculations reflect the local maximum in the series, placed on the excited level $4d4p$. At present it is the

TABLE IV. Excitation energies and autoionization widths of the ^1P states in Ca below the $3d$ threshold.

	Energies (eV)			Widths (meV)			
	Theory		Expt.	Theory		Expt.	
Level	Present	Ref. [37]	Ref. [38]	Present	Ref. [37]	Ref. [39]	Ref. [40]
$3d5p$	6.604	6.633	6.583	70.2	84.6	76.2	62.9
$3d6p$	7.038	7.080	7.024	5.6	6.7	8.6	6.3
$3d7p$	7.342	7.415	7.339	50.9	39.9	34.1	
$3d8p$	7.471	7.502	7.476	23.2	31.5	19.8	
$3d9p$	7.556	7.575	7.559	14.1	28.2	12.4	
$3d10p$	7.614	7.624	7.617	10.1	20.7	9.9	
$4p5s$	7.166	7.300	7.186	139	13.2	71.0	
$3d4f$	6.938	6.960	6.936	0.004	0.1		
$3d5f$	7.248	7.260	7.254	2.8	0.3	3.4	
$3d6f$	7.427	7.427	7.424	1.4	2.4		
$3d7f$	7.529	7.527	7.528	1.1	0.7		
$3d8f$	7.596	7.593	7.595	0.8	0.6		

most exact theoretical calculation.

In the work of Froese-Fischer and Hansen [32] oscillator strengths are obtained within the framework of the many-configuration HF method, also in a frozen-core approximation, but without polarization. These calculations provide much less accurate results for the values of oscillator strengths and their distribution over a series. The difference between these data and our data characterizes the importance of core polarization in the case of Ca. However, in this case it is important also to account for the dependence on the orbital momentum of the valence electron. This is illustrated by comparison with the results of Victor, Stewart, and Laughlin [34], where only one variational parameter in expression (3.1) was used. As a result, although oscillator strengths improved, they still greatly differed from experimental values. This is associated with the "dip" of the $3d$ orbital in Ca^+ and its strong dependence on details in screening. We also note that *ab initio* calculations of $4s^2$-$4s4p$ ^1P oscillator strengths by Glass [36] with a full account of the correlation between core and valence electrons give values $f_L=1.97$, $f_V=1.76$. This is much worse than our present calculations and it indicates that at present the usage of semiempirical core potential is more suitable.

More sensitive to correlation corrections are the autoionizing widths. Comparison with experimental data in Table IV shows that our method yields a satisfactory accuracy for the widths in the ^1P series, except for the perturber level $4p5s$. Its width is very sensitive to the configuration-mixing parameter, which in turn strongly depends on the details of calculating the strong interaction of the $4p5s$ state with the $3dnp$ series; e.g., on basis size, adjustable parameters in $V_{\rm pol}$, and on handling the nonphysical states. Our method is somewhat unstable for calculating the width of such states. Scott *et al.* [37] computed the AIS ^1P series of Ca using the R-matrix approach, which allows for configuration mixing and direct inclusion of core polarization. These calculations are much more laborious but do not lead to a considerable improvement in comparison with our calculations, and in some cases give even worse results. For example, the width of the $4p5s$ state is five times narrower than the experimental value. On a balance we expect our widths to be uncertain within a factor of 2.

In Table V we present the AIS parameters for Ca below the $5s$ threshold that were used in calculations of the resonance excitation cross section for the $4s$-$4p$ transition by the DM. Here only AIS's with total terms $^{1,3}S$, $^{1,3}P$, $^{1,3}D$, and $^{1,3}F$ were considered. No data for direct comparison of obtained parameters exist, as far as we know, though their accuracy can be assessed in analogy with our discussion of the ^1P series. In Table V positions and full widths of the AIS's along with relative widths w_i are given, which are defined as

$$w_i=\left[\sum_{l_i}\Gamma_{l_i}\right]\Big/\Gamma\ . \tag{5.2}$$

Because the orbital momentum l_i of the electron scattered in channel i cannot be observed (only the target state can be) the values w_i are more useful than the partial widths Γ_{l_i}. Comparison of the values w_i shows that it is impossible to associate any dominant decay channel with most AIS's. It is possible only to note some preference of decay channels connected with the $4p$ level. In Table V the coefficients C_1 of the dominant basis function in a multiconfiguration expansion (5.1) are presented, on the basis of which the classification of AIS's was carried out. As most values of C_1 are not sufficiently large, it is evident that in these cases the classification in terms of configurations is only for the sake of convenience.

VI. RESONANCE STRUCTURE

The scattering and AIS parameters calculated in previous chapters yield the resonance structure in the $4s$-$4p$ cross section of Ca^+ within the DM according to Eq. (2.13). Such calculations were carried out in the energy region from the $4p$ excitation threshold (0.231 Ry) up to the nearest $5s$ level (0.475 Ry). Resonance contributions were accounted for in all partial waves for $L=0,1,2,3$. It should be noted that in practical applications the following equation is often used instead of relation (2.13):

$$T=T^0+2i\sum_{\mu}\frac{\alpha_\mu\alpha_\mu}{E-\varepsilon_\mu+\Delta_\mu+\frac{i}{2}\Gamma_\mu}\ , \tag{6.1}$$

where

$$\Gamma_\mu\equiv\Gamma_{\mu\mu},\quad \Delta_\mu\equiv\Delta_{\mu\mu}\ ,$$

which may be obtained, assuming that neighboring resonances do not overlap, which is true for weakly interacting resonances. However, the control calculations have shown that for Ca^+ these two expressions give very different results in a number of cases, i.e., the assumption is not justified, and therefore we have used expression (2.13). Although the DM eliminates the AIS interaction through the continuum, this interaction is partially accounted for in Eq. (2.13) to the extent, for example, to which different scattering channels in the unitarized distorted-wave method couple in comparison with the CCM.

For (2.13) one needs the energy dependence upon all the quantities in (2.14)–(2.16). But unlike (2.13) with its explicit strong energy dependence in the vicinity of resonances they vary only very slowly with energy. Hence all parameters in (2.14)–(2.16) were calculated at five equidistantly spaced energies, as mentioned above, interpolating them when calculating the resonance structure of the excitation cross section on the fine-energy mesh of 0.001 eV. It shows the main advantage of the DM in comparison with the CCM where it is necessary to perform cumbersome calculations in every energy point.

The resonance excitation cross section of the transition $4s_{1/2}$-$4p_{1/2}$ in Ca^+ is shown in Fig. 2. In Fig. 2 only well-resolved resonances are shown. It follows from Fig. 2 that resonances lead to considerable changes in the near-threshold region of cross sections. The resonance structure differs greatly from that of the 6CC calculations [8], where only broad resonances are seen, due likely to the relatively large energy mesh (0.01 Ry). Good agree-

TABLE V. Energies, total and partial widths and configuration mixing parameters of autoionizing states in Ca below the 5*s* threshold.

Level	*E* (eV)	*G* (meV)	4*sEl* (%)	3*dEl* (%)	4*pEl* (%)	*C* (%)
$5s^2\,{}^1S$	3.689	63.7	41.3	52.1	6.6	87.8
$5s5p\,{}^3P$	4.276	31.7	4.1	30.9	65.0	84.9
$5s4d\,{}^3D$	4.336	75.1	19.3	19.2	61.5	84.2
$5s4d\,{}^1D$	4.394	231.0	16.9	8.2	74.9	77.7
$5s5p\,{}^1P$	4.611	35.4	19.5	24.6	55.9	71.3
$4d5p\,{}^3F$	4.948	72.1	0.1	37.0	62.9	76.5
$4d^2\,{}^1D$	4.971	123.0	0.7	53.0	46.3	77.8
$4d^2\,{}^1S$	4.984	134.0	4.0	41.5	54.5	61.8
$5s6s\,{}^3S$	5.110	3.5	15.3	0.6	84.1	93.7
$4d5p\,{}^1F$	5.118	121.0	6.6	35.5	57.9	52.5
$5s6s\,{}^1S$	5.255	64.1	25.4	41.5	33.1	89.0
$4d5p\,{}^3P$	5.280	82.8	9.4	34.2	56.4	80.2
$4d5p\,{}^1P$	5.340	51.2	12.3	30.5	57.2	24.4
$5s5d\,{}^1D$	5.431	58.8	18.9	9.5	71.6	92.5
$5s5d\,{}^3D$	5.437	13.2	31.8	15.2	53.0	92.4
$5s6p\,{}^3P$	5.454	17.7	11.9	32.2	55.9	91.6
$5s4f\,{}^3F$	5.513	7.9	33.4	13.5	53.1	81.5
$5s4f\,{}^1F$	5.651	38.4	5.0	28.1	66.9	61.3
$5p^2\,{}^1D$	5.664	68.2	0.8	22.1	77.2	56.1
$5s6p\,{}^1P$	5.666	91.1	15.7	32.9	51.4	62.3
$5s7s\,{}^3S$	5.711	18.2	18.7	0.5	80.8	97.4
$5s7s\,{}^1S$	5.754	32.1	31.8	30.5	37.7	95.1
$4d6s\,{}^3D$	5.799	7.7	5.6	31.8	62.6	71.5
$4d6s\,{}^1D$	5.819	4.5	5.6	13.1	81.3	41.3
$5s5f\,{}^3F$	5.836	4.5	49.7	40.5	9.8	78.5
$5s7p\,{}^3P$	5.854	4.6	12.0	33.8	54.2	97.1
$5s5f\,{}^1F$	5.876	8.4	17.1	12.3	70.6	75.6
$5s6d\,{}^3D$	5.882	16.7	28.2	28.7	43.1	80.8
$5s7p\,{}^1P$	5.887	29.7	20.2	34.3	45.5	83.9
$5s6d\,{}^1D$	5.922	51.6	22.3	11.2	66.5	43.9
$4d4f\,{}^3F$	5.961	23.1	0.9	34.6	64.5	60.4
$5s8s\,{}^3S$	5.980	0.5	41.9	6.3	51.8	88.3
$4d6p\,{}^3P$	5.982	6.3	1.1	32.5	56.7	50.0
$5s8s\,{}^1S$	5.998	41.0	15.9	26.6	57.5	91.2
$4d5d\,{}^3S$	5.998	2.2	0.1	17.4	82.5	71.0
$5p6s\,{}^1P$	6.013	16.7	9.6	36.5	53.9	39.7
$4d5d\,{}^3D$	6.026	1.5	4.1	28.4	67.5	88.9
$5s6f\,{}^1F$	6.042	9.3	13.8	40.9	45.3	83.2
$5s6f\,{}^3F$	6.048	15.4	5.2	29.2	65.6	73.7
$5s8p\,{}^3P$	6.055	3.1	6.3	34.4	59.3	98.1
$4d4f\,{}^1F$	6.063	5.5	2.2	41.0	56.8	41.2
$5s7d\,{}^3D$	6.063	5.1	34.4	21.4	44.3	97.7
$5s8p\,{}^1P$	6.069	4.7	30.9	26.9	42.2	84.0
$5s7d\,{}^1D$	6.069	14.8	32.4	11.5	56.1	97.1
$5p^2\,{}^1S$	6.075	187.0	1.6	25.6	72.6	32.8
$5s9s\,{}^3S$	6.130	0.7	17.9	0.4	81.7	99.2
$4d6p\,{}^3F$	6.137	3.8	2.7	49.3	48.0	39.6
$5s9s\,{}^1S$	6.141	3.6	66.0	9.5	24.5	89.6
$5s7f\,{}^1F$	6.158	6.3	14.5	42.3	43.2	92.0
$5s9p\,{}^3P$	6.171	2.6	5.4	36.1	58.5	95.9
$4d5d\,{}^1D$	6.171	23.1	3.5	68.0	28.5	59.5
$5s9p\,{}^1P$	6.174	1.5	35.1	27.9	37.0	94.4
$5s8d\,{}^3D$	6.177	2.5	38.2	19.1	42.7	99.1
$5s8d\,{}^1D$	6.183	26.8	6.3	28.0	65.7	66.6
$5s7f\,{}^3F$	6.195	2.8	12.7	29.0	58.3	72.7
$4d5d\,{}^1S$	6.217	6.3	44.1	5.7	50.2	65.7
$5s10s\,{}^3S$	6.223	0.5	20.8	0.4	78.8	99.5
$5s8f\,{}^1F$	6.233	6.5	9.7	40.7	49.6	91.6
$4d4f\,{}^1P$	6.223	41.3	7.5	29.5	63.0	23.0

TABLE V. (*Continued*).

Level	E (eV)	G (meV)	$4sEl$ (%)	$3dEl$ (%)	$4pEl$ (%)	C (%)
$5s10p\ ^3P$	6.237	8.5	8.0	31.5	60.5	67.4
$5s10p\ ^1P$	6.245	0.4	42.0	27.7	30.3	95.4
$5s9p\ ^3D$	6.250	1.4	40.0	17.1	42.9	99.4
$5s9d\ ^1D$	6.251	4.3	28.6	7.4	64.0	99.1
$5s8f\ ^3F$	6.253	3.8	16.1	18.0	65.9	90.1
$5s10s\ ^1S$	6.261	7.2	0.6	21.7	77.7	27.4
$4d4f\ ^3P$	6.263	10.3	11.7	27.2	61.2	30.3
$5s9f\ ^1F$	6.296	12.5	6.4	35.2	58.4	77.4
$5p6s\ ^3P$	6.322	2.2	0.9	25.9	68.5	23.4
$5s9f\ ^3F$	6.329	7.7	17.8	15.9	66.3	89.7
$4d6p\ ^1F$	6.365	11.1	9.0	15.3	75.7	26.3
$4d7s\ ^3D$	6.373	8.6	13.4	33.3	53.3	89.0
$4d6p\ ^1P$	6.374	14.0	26.0	29.3	50.7	30.5
$4d7s\ ^1D$	6.387	26.3	17.9	10.3	71.8	85.3
$4d5f\ ^3F$	6.421	23.3	0.9	16.7	82.4	76.2

ment with the 6CC calculations was obtained only in the region of the first maximum due to resonances with $5s5p$ and $5s4d$ configurations (see Table V). One of the reasons for this discrepancy is the difference of background cross sections in the DM and 6CC calculations, as mentioned above. The largest differences are observed in the region above 5 eV, where according to the current resonance structure calculations a broad $4d5p\ ^1F$ resonance dominates, but the 6CC calculations show a destructive dip. A similar situation is observed also in the region of the $5s6d$ and $5s7d$ resonances at energies between 5.8 and 5.9 eV. A more detailed analysis of the reasons for this disagreement with 6CC calculations needs to examine the partial cross sections.

In Fig. 3 the calculations are compared with experimental data, where the $4s_{1/2}$-$4p_{3/2}$ excitation cross section is shown folded with the spread of a beam with a half-width of 0.15 eV for our calculations and with a half-width of 0.3 eV for the 6CC calculations. These half-widths are characteristic in the near-threshold region for experimental measurements of Refs. [1] and [2]. Such folding greatly reduces the average swing of resonances in excitation cross sections, which lies within the error of the experiments. Though in these experiments some faint structure is observed, experimental errors do not allow one to interpret it unambiguously. In the more elaborate and precise measurements of Frontov [10] this resonance structure is clearly resolved and a near-threshold cross section greatly differs from the previous experiments. Somewhat doubtful is the rather large absolute value of the excitation cross section obtained by Frontov in the near-threshold region, as it considerably exceeds not only our and the 6CC calculations, but also earlier measurements, even by taking into account their errors. The experimentally measured resonance structure [10] agrees

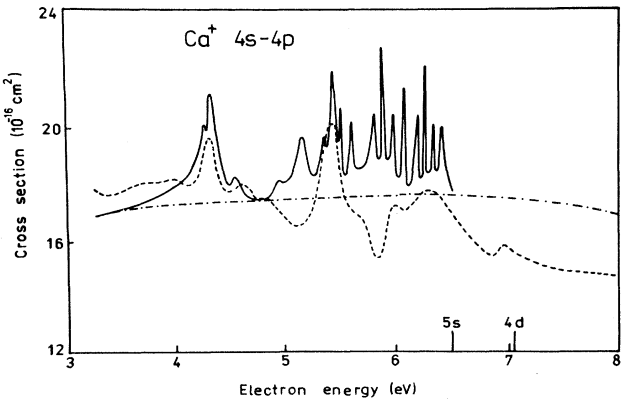

FIG. 2. Resonance structure in the excitation cross section of the Ca^+ $4p_{3/2}$ states: ——, present results, DM model; — — — 6CC results, Mitroy *et al.* (1988); —·—·—·, present results, nonresonant 3CC model.

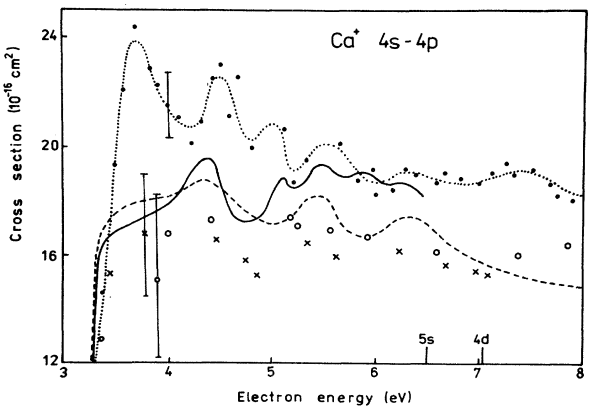

FIG. 3. Comparison of the theoretical excitation cross section of the Ca^+ $4p_{3/2}$ state convoluted over the energy resolution function with experimental data: ——, present results, convoluted with an energy resolution width of 0.15 eV; — — —, 6CC results of Mitroy *et al.*, convoluted with a width of 0.3 eV. The experimental data of Refs. [1,2,10] are depicted as ×, ○, and ●, respectively; · · · ·, digital processing of the experimental data of Frontov (1985).

qualitatively with current calculations and 6CC calculations only in the region above 4 eV. According to our calculations, as shown in Table V, there is only one resonance $5s^2\,{}^1S$ in the threshold region, which could not lead to such a sharp resonance structure because of the weakness of the ^1S partial wave. Nor do calculations by Mitroy *et al.* [8] confirm the existence of a dominant maximum at the $4s$-$4p$ excitation threshold. This maximum is not the result of AIS influence but is caused perhaps by a sharp increase of the direct nonresonance excitation cross section in a threshold, decreasing as energy goes up. Such behavior is probably due to the interaction of the projectile electron with the core. This maximum is seen also, though it is less noticeable, in scattering by Mg^+ [41], and is very clearly seen in the case of scattering by Sr^+ [42] and Ba^+ [43], i.e., it is enhanced with an increase of the core.

VII. SUMMARY

We have calculated the $4s$-$4p$ excitation cross sections within the DM and have shown that resonances play an important role in the near-threshold region of Ca^+ excitation. Our calculations illustrate the effectiveness of the diagonalization method, the accuracy of which is compared with much more cumbersome, direct methods for strong coupling and which, at the same time, allow us to obtain the detailed characteristics of the process of scattering and AIS's. These characteristics may then be used for calculating other scattering processes, e.g., photoionization of the Ca atom.

These calculations and those of Mitroy *et al.* [8] and Zatsarinny [9] completely resolve the large discrepancy between theoretical and experimental resonant excitation cross sections of heavy alkaline-earth ions in the near-threshold region that are caused by core polarization. Nevertheless, considerable difficulties remain in modeling the resonance structure in experimental measurements by Frontov [10]; details of the interaction of the projectile electron with a many-electron core are not described fully adequately within the model of simple semiempirical polarization core potential. It would be desirable to carry out further investigations that are both theoretical and experimental.

ACKNOWLEDGMENTS

We are grateful to Dr. A. I. Imre for stimulating the present work and for many useful discussions on experimental scattering data. Most of the calculations were carried out on the EC-1036 computer at the Central Statistical Department in Uzhgorod, and we wish to thank the employees of this department for assistance with the execution of the calculations.

[1] P. O. Taylor and G. H. Dunn, Phys. Rev. A **8**, 2304 (1973).
[2] I. P. Zapesochnyi, V. A. Kel'man, A. I. Imre, A. I. Dashchenko, and F. F. Danch, Zh. Eksp. Teor. Fiz. **69**, 1948 (1975) [Sov. Phys.—JETP **42**, 989 (1975)].
[3] P. G. Burke and D. L. Moores, J. Phys. B **1**, 575 (1968).
[4] A. Burgess and V. P. Sheorey, J. Phys. B **7**, 2403 (1974).
[5] J. V. Kennedy, V. P. Myerscough, and M. R. C. McDowell, J. Phys. B **11**, 1303 (1978).
[6] M. Chidichimo, J. Phys. B **14**, 4149 (1981).
[7] A. Z. Msezane, J. Phys. B **21**, L61 (1988).
[8] J. Mitroy, D. C. Griffin, D. W. Norcross, and M. S. Pindzola, Phys. Rev. A **38**, 3339 (1988).
[9] O. I. Zatsarinny, V. I. Lengyel, and E. A. Masalovich, Opt. Spectrosc. **67**, 20 (1989).
[10] V. I. Frontov, Opt. Spectrosc. **59**, 460 (1985).
[11] V. V. Balashov, S. I. Grishanova, I. M. Kruglova, and V. S. Senashenko, Opt. Spectrosc. **28**, 859 (1970).
[12] M. I. Gaysak, V. I. Lengyel, V. T. Navrotsky, and E. P. Sabad, Ukr. Fiz. Zh. **27**, 1617 (1982).
[13] V. I. Lengyel, V. T. Navrotsky, and E. P. Sabad, J. Phys. B **23**, 2847 (1990).
[14] S. M. Kazakov, V. I. Lengyel, E. A. Masalovich, E. P. Sabad, D. V. Christophorov, and I. J. Cherlenyak, Ukr. Fiz. Zh. **30**, 502 (1985).
[15] V. I. Lengyel, V. T. Navrotsky, and E. P. Sabad, Usp. Fiz. Nauk **151**, 425 (1987) [Sov. Phys.—Usp. **30**, 220 (1987)].
[16] K. Smith and L. A. Morgan, Phys. Rev. **165**, 110 (1968).
[17] D. W. Norcross and M. J. Seaton, J. Phys. B **9**, 2983 (1976).
[18] W. Muller, J. Flesh, and W. Meyer, J. Chem. Phys. **80**, 3297 (1984).
[19] C. Froese-Fischer, Comput. Phys. Commun. **14**, 145 (1978).
[20] A. A. Radtsig and B. M. Smirnov, *Handbook on Atomic and Molecular Physics* (Atomizdat, Moscow, 1980), p. 79.
[21] S. Bashkin and J. O. Stoner, *Atomic Energy Levels and Grotrian Diagrams* (North-Holland, Amsterdam, 1975), Vol. 3.
[22] C. Laughlin and G. A. Victor, Adv. At. Mol. Phys. **25**, 163 (1988).
[23] L. B. Bersuker, Opt. Spectrosc. **3**, 97 (1957).
[24] A. S. Gallagher, Phys. Rev. **157**, 24 (1967).
[25] B. Emmoth, M. Braun, J. Bromander, and I. Martinson, Phys. Scr. **12**, 220 (1975).
[26] M. A. Crees, M. J. Seaton, and P. M. H. Wilson, Comput. Phys. Commun. **15**, 23 (1978).
[27] U. Fano, Phys. Rev. **140**, A67 (1965).
[28] P. G. Burke, Comput. Phys. Commun. **1**, 241 (1969).
[29] A. Hibbert, Comput. Phys. Commun. **1**, 359 (1969).
[30] L. Lipsky and A. Russek, Phys. Rev. A **142**, 59 (1966).
[31] O. Robaux, J. Phys. B **21**, 3167 (1988).
[32] C. Froese-Fischer and J. E. Hansen, J. Phys. B **18**, 4031 (1983).
[33] J. Sugar and C. Corliss, J. Phys. Chem. Ref. Data **8**, 875 (1979).
[34] G. A Victor, R. F. Stewart, and C. Laughlin, in *Beam-Foil Spectroscopy,* edited by I. A. Seliin and D. J. Pegy (Plenum, New York, 1976), Vol. 1, p. 43.
[35] W. H. Parkinson, E. M. Reeves, and F. S. Tomkins, J. Phys. B **9**, 157 (1976).
[36] R. Glass, J. Phys. B **18**, 4047 (1985).
[37] P. Scott, A. E. Kingston, and A. Hibbert, J. Phys. B **16**, 3945 (1983).
[38] C. M. Broun, S. G. Tilford, and M. L. Ginter, J. Opt. Soc.

Am. **63**, 1454 (1973).
[39] R. W. Ditchburn and R. D. Hudson, Proc. R. Soc. London **256**, 53 (1960).
[40] G. H. Newson, Proc. Phys. Soc. London **87**, 975 (1966).
[41] I. P. Zapesochny, A. I. Dashchenko, V. I. Frontov, A. I. Imre, A. N. Gomonay, V. I. Lengyel, V. T. Navrotsky, and E. P. Sabad, Pis'ma Zh. Eksp. Teor. Fiz. **39**, 45 (1984) [JETP Lett. **39**, 51 (1984)].
[42] V. I. Frontov, A. I. Dashchenko, A. I. Imre, I. P. Zapesochny, and A. N. Gomonay, in *Proceedings of the 11th Soviet Conference on Electronic and Atomic Collisions (Riga, 1984),* edited by R. Damburg (Institute of Physics of the Latvian Academy of Science, Riga, 1984), Vol. 2, p. 33.
[43] V. I. Frontov, A. I. Dashchenko, A. I. Imre, and I. P. Zapesochny, Ukr. Fiz. Zh. **30**, 833 (1985).